Real-time imaging of spin-to-orbital angular momentum hybrid remote state preparation

Manuel Erhard,[1,*] Hammam Qassim,[1] Harjaspreet Mand,[1] Ebrahim Karimi,[1,†] and Robert W. Boyd[1,2]

[1]*Department of Physics, University of Ottawa, 150 Louis Pasteur, Ottawa, Ontario, Canada K1N 6N5*

[2]*Institute of Optics, University of Rochester, Rochester, New York 14627, USA*

(Received 29 April 2014; published 10 August 2015)

There exists two prominent methods to transfer information between two spatially separated parties, namely Alice (A) and Bob (B): quantum teleportation and remote state preparation. However, the difference between these methods is, in the teleportation scheme, the state to be transferred is completely unknown, whereas in state preparation it should be known to the sender. In addition, photonic state teleportation is probabilistic due to the impossibility of performing a two-particle complete Bell-state analysis with linear optics, while remote state preparation can be performed deterministically. Here we report the first realization of photonic hybrid remote state preparation from spin to orbital angular momentum degrees of freedom. In our scheme, the polarization state of photon A is transferred to orbital angular momentum of photon B. The prepared states are visualized in real time by means of an intensified CCD camera. The quality of the prepared states is verified by performing quantum state tomography, which confirms an average fidelity higher than 99.4%. We believe that this experiment paves the way towards a novel means of quantum communication in which encryption and decryption are carried out in naturally different Hilbert spaces, and therefore may provide a means for enhancing security.

DOI: 10.1103/PhysRevA.92.022321 PACS number(s): 03.67.Hk, 42.50.−p, 03.67.Bg

I. INTRODUCTION

Entanglement is an intriguing aspect of quantum mechanics that lies at the heart of the Einstein-Podolsky-Rosen (EPR) paradox [1], Hardy paradox [2], and Leggett inequalities [3]. The processes enabled by entanglement are teleportation and remote state preparation (RSP) of quantum states. In general, a quantum teleportation scheme entails the transfer of an arbitrary *unknown* quantum state between two spatially separated participants. In contrast to teleportation, the RSP protocol needs knowledge of the state to be transmitted. In 1993, the first quantum state teleportation scheme based on three spin-half particles [4] was proposed, and seven years later the first remote state preparation scheme [5] was presented. The RSP scheme has been realized experimentally by means of two entangled particles and different degrees of freedom (DOFs) [6], and hyperentangled photons [7] in which nonclassical information is transferred between two separate parties. However, experimental realization of teleportation protocols is probabilistic, as performing complete Bell-state measurements involving two particles and one DOF is impossible, when using linear optics [8]. But schemes using different DOFs, such as that of RSP, can be deterministic. Furthermore, combining different DOFs of a single particle provides a novel way to perform high-dimensional quantum key distribution [9], superdense coding [10], quantum metrology [11], and high-dimensional quantum teleportation [12]. Spin and orbital angular momentum (OAM) of light, associated respectively with the vectorial nature and helical phase fronts of optical beams, are thoroughly examined DOFs, and the radial index of Laguerre-Gauss modes has recently been investigated [13]. However, a hybrid RSP experiment from spin to OAM of light remains unrealized.

In this article, we show experimentally how to remotely prepare a polarization state of one photon to a different Hilbert space, here the OAM, of its entangled partner photon. Our implemented RSP scheme is a merger of two different proposals reported in Refs. [14,15]. Transmission of the quantum state from polarization to the OAM DOF also shows experimentally that quantum information can be transmitted between completely different physical properties of spatially separated particles, provided they are entangled.

II. EXPERIMENTAL METHOD

Photon pairs entangled in position and anticorrelated in momentum space (EPR states) can be generated via spontaneous parametric down conversion (SPDC) in a collinearly phase matched, type-I β-barium borate (BBO) crystal. As a consequence of conservation of the OAM, the SPDC photons are in a superposition of negative and positive OAM states, since the Gaussian pump beam does not carry a net OAM [16]. Thus the SPDC state can be written as [17]

$$|\chi\rangle = \sum_{\ell=0}^{\infty} c_\ell(|-\ell\rangle_A|+\ell\rangle_B + |+\ell\rangle_A|-\ell\rangle_B) \otimes |H\rangle_A|H\rangle_B, \tag{1}$$

where the constant c_ℓ depends on crystal and pump properties and $|\ell\rangle_i$ is the OAM state of photon i, which is ℓ in the direction of propagation in units of $\hbar$—the reduced Planck constant [18]. $|H\rangle$ and $|V\rangle$ refers to horizontal and vertical polarization of photon A or B. Charlie (C), who in principle can be different from Alice, then prepares an arbitrary state in the polarization DOF of photon A to be transferred to B; see Fig. 1. The polarization states of photons A and B are in a product state as shown in Eq. (1), i.e., $|H\rangle_A|H\rangle_B$. The arbitrary SU(2) polarization transformation of photon A performed by Charlie is given by $|H\rangle_A \to \alpha|H\rangle_A + \beta|V\rangle_A$, where α and β are arbitrary complex numbers with $|\alpha|^2 + |\beta|^2 = 1$. To see the action of a Bell-state measurement on the SPDC state $|\chi\rangle$ after Charlie's polarization transformation, we define the

*Also at Faculty of Physics, University of Vienna, Boltzmanngasse 5, A-1090 Vienna, Austria.

†ekarimi@uottawa.ca

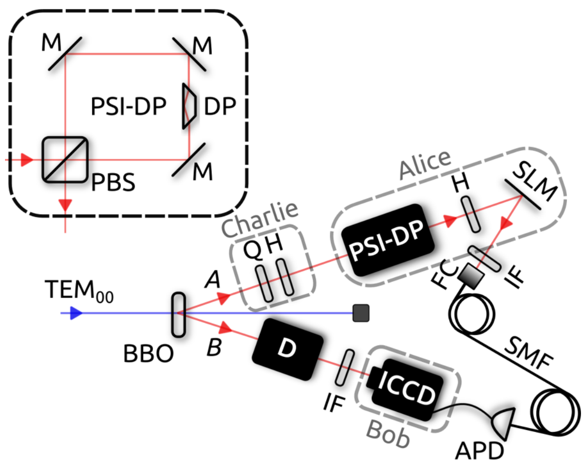

FIG. 1. (Color online) Quasi-cw 150 mW UV laser (355 nm, repetition rate 100 MHz, TEM$_{00}$ mode) pumps a phase-matched, type-I BBO crystal. The generated photon pairs are entangled in their OAM DOF. Charlie controls the orientations of the QWP (Q) and HWP (H), which allows him to place photon A in an arbitrary polarization state. The polarizing Sagnac interferometer containing a Dove prism (PSI-DP), shown in the inset, in combination with the HWP, spatial light modulator (SLM), bandpass interference filter (IF), and single mode optical fiber (SMF) perform the Bell-state measurement [20]. The HoloEye Pluto SLM diffracts only horizontally polarized photons, acting as a polarizer. An SLM with a proper hologram and a SMF postselect the OAM Hilbert subspace: only photons with a flattened wavefront ($|\ell| = 0$) can propagate efficiently through an SMF. The photons couple via a fiber coupler (FC) into the SMF for detection by an avalanche photon diode (APD). The detector (APD) triggers the ICCD camera to record the spatial distribution of photon B. Photons are filtered with 10 nm IFs before the detector and ICCD camera for noise reduction. During the preparation and measurement of photon A, photon B propagates in delay line (D), compensating for electronic delay. To measure the fidelity of the transported state, the ICCD camera is replaced by another SLM and the coincidence counts between A's and B's detectors are measured.

four Bell states for a single photon, but in two bidimensional Hilbert spaces of polarization $\{|H\rangle,|V\rangle\}$ and OAM subspace of $\{|+\ell\rangle,|-\ell\rangle\}$:

$$|\Phi_\ell^{\pm}\rangle_A = \frac{1}{\sqrt{2}}(|h_\ell,H\rangle_A \pm |v_\ell,V\rangle_A),$$
$$|\Psi_\ell^{\pm}\rangle_A = \frac{1}{\sqrt{2}}(|v_\ell,H\rangle_A \pm |h_\ell,V\rangle_A), \tag{2}$$

where the first and second positions inside the ket represent the OAM and polarization states of photon A, respectively, and $|h_\ell\rangle = (|+\ell\rangle + |-\ell\rangle)/\sqrt{2}$ and $|v_\ell\rangle = -i(|+\ell\rangle - |-\ell\rangle)/\sqrt{2}$ refer to the horizontal and vertical basis in the OAM subspace of $\{|+\ell\rangle,|-\ell\rangle\}$ [19]. The Bell states are mutually orthogonal and form a complete basis in the spin-OAM Hilbert space of $\{|+\ell,H\rangle,|-\ell,H\rangle,|+\ell,V\rangle,|-\ell,V\rangle\}$. Thus we rewrite Eq. (1) in terms of the spin-OAM Bell states of Eq. (2):

$$|\chi\rangle = \frac{1}{2}\sum_{\ell=0}^{\infty} c_\ell\{|\Phi_\ell^{+}\rangle_A(\alpha|h_\ell\rangle_B + \beta|v_\ell\rangle_B)$$
$$+ |\Phi_\ell^{-}\rangle_A(\alpha|h_\ell\rangle_B - \beta|v_\ell\rangle_B) + |\Psi_\ell^{+}\rangle_A(\alpha|v_\ell\rangle_B + \beta|h_\ell\rangle_B)$$
$$+ |\Psi_\ell^{-}\rangle_A(\alpha|v_\ell\rangle_B - \beta|h_\ell\rangle_B)\}|H\rangle_B, \tag{3}$$

where we used $|\pm\ell\rangle = (|h_\ell\rangle \pm i|v_\ell\rangle)/\sqrt{2}$. Equation (3) shows that if A performs one of the Bell-state measurements defined in Eq. (2), the state of photon B is left in a superposition of orthogonal OAM modes with the coefficients determined by the polarization state of photon A. Consequently, the polarization state of photon A determines the state of photon B, but in the OAM space. Assuming a fixed OAM basis, B applies one of the unitary operators from the set: $\{\hat{\mathbb{1}},\hat{\sigma}_x,i\hat{\sigma}_y,\hat{\sigma}_z\}$ to photon B's OAM state based on the outcome of A's Bell-state measurement.

Projection of photon A onto one of the four single-photon spin-OAM Bell states, i.e., $|\Phi^{\pm}\rangle, |\Psi^{\pm}\rangle$, is achieved by a Sagnac based interferometer (Fig. 1, inset), a half-wave plate (HWP), and a spatial light modulator (SLM) [20]. The polarizing Sagnac interferometer containing a Dove prism (PSI-DP) couples photon spin to photon OAM. Since the photon is collimated within the interferometer, the DP transformation is effectively acting only on the OAM space; $\mathrm{DP}_{\pm\theta}\cdot|\pm\ell\rangle \rightarrow e^{\pm 2i\ell\theta}|\mp\ell\rangle$, where $\pm\theta$ is the rotational angle of the DP with the sign reference to the propagation direction [21,22]. The polarizing beam splitter (PBS) at the entry of the PSI-DP converts the incoming photon state into a superposition of two counterpropagating horizontally and vertically polarized states. The rotated DP causes these counterpropagating beams to accumulate a relative phase difference of $|4\ell\theta|$. By setting $\theta = \pi/(8\ell)$, the PSI-DP transforms each of the four Bell states according to

$$|\Phi^{+}\rangle \rightarrow |v_\ell,A\rangle, \quad |\Phi^{-}\rangle \rightarrow |v_\ell,D\rangle,$$
$$|\Psi^{+}\rangle \rightarrow |h_\ell,A\rangle, \quad |\Psi^{-}\rangle \rightarrow |h_\ell,D\rangle, \tag{4}$$

where unnecessary global phases are omitted and A (D) refer to the antidiagonal (diagonal) state of polarization. It is worth mentioning that a liquid crystal q-plate implemented with appropriate wave plates and a PBS can also sort all spin-OAM Bell states [23]. In order to project the state of photon A onto one of the Bell states, the outgoing photons from PSI-DP must be projected onto the transformed states given in Eq. (4). A $\pi/8$-rotated HWP, an SLM, and a single mode optical fiber (SMF) can project onto the h_ℓ or v_ℓ states. The SLM displaying the desired hologram, in conjunction with the SMF, selects a definite OAM subspace $|\ell|$. This requires very precise aligning of both the near and far field of two counterpropagating beams inside the PSI-DP such that the centers of the SMF, the hologram, and the SPDC source are precisely superimposed. Unlike for the case of multiparticle Bell states, by employing single particle hybrid Bell states it is possible to perform a complete Bell-state measurement deterministically and with 100% efficiency [24,25]. To project on any one of the four Bell states a proper setting of the HWP and SLM following the PSI-DP is necessary. Here we choose to project onto the

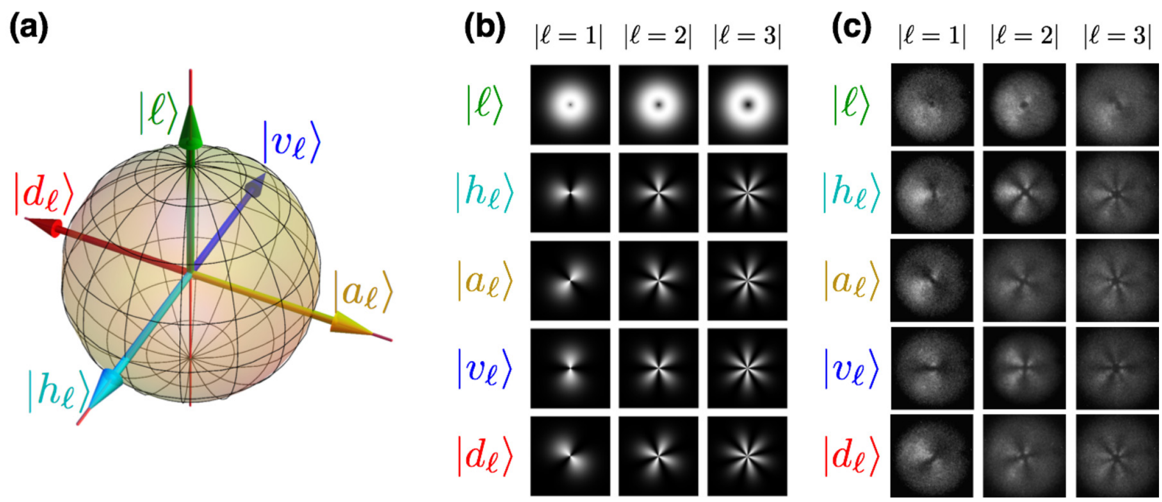

FIG. 2. (Color online) Qualitative comparison of experimental data and theoretical predictions. (a) Pictorial representation of the prepared states on the OAM Poincaré sphere. South and north poles represent the $|+\ell\rangle$ and $|-\ell\rangle$-states, respectively, and an equal superposition of $|+\ell\rangle$ and $|-\ell\rangle$ stands on the equator. (b) Theoretically predicted spatial distributions of the prepared states corresponding to initial polarization states of Charlie being set to circular-left $|L\rangle \to |\ell\rangle$, horizontal $|H\rangle \to |h_\ell\rangle$, antidiagonal $|A\rangle \to |a_\ell\rangle$, vertical $|V\rangle \to |v_\ell\rangle$, and diagonal $|D\rangle \to |d_\ell\rangle$. (c) Experimentally recorded spatial distributions of photon B on the ICCD camera conditioned by detecting photon A in the spin-orbit Bell state of $|\Phi_\ell^+\rangle$. Total exposure time per picture is 600 s with a time window of 4 ns.

$|\Phi_\ell^+\rangle$ state because it requires no additional operation by B, and leaves B's photon in a superposition of OAM states described by Eq. (3), i.e., $|\chi\rangle_B = {}_A\langle\Phi_\ell^+|\chi\rangle \propto \alpha|h_\ell\rangle_B + \beta|v_\ell\rangle_B$. In other words, when $|\Phi_\ell^+\rangle$ is measured and the detector fires, B finds his photon in the state $\alpha|h_\ell\rangle_B + \beta|v_\ell\rangle_B$, with the same coefficients α and β as in the unknown polarization state.

In the paraxial approximation the $|\pm\ell\rangle$ states can be represented by Laguerre-Gauss modes, i.e., $\langle\mathbf{r}|\pm\ell\rangle \propto \exp(\pm i\ell\varphi)$, where φ is the azimuthal angle in polar coordinates. Due to the postselection introduced by the SMF, only the lowest radial p-index mode ($p = 0$) contributes. The theoretical prediction of the spatial distribution of B's photons on the ICCD camera is plotted in Fig. 2(b). To ensure that the entangled partner photon of A is captured by the camera, photon A is guided via an SMF to a single photon detector, which generates an electronic signal that triggers the ICCD camera (Andor iStar 1024×1024). While the pump laser repetition rate (100 MHz) dictates that the maximum time window for capturing B's photon is 10 ns, we chose the detection time window of the ICCD camera to be 4 ns to diminish noise. The delay line compensates for the electronic delay between the detector and ICCD camera ($\sim$100 ns); see Refs. [26,27] for more details on the camera settings. While photon B is propagating in the delay line, Charlie prepares the state which Alice is going to transfer to Bob.

III. EXPERIMENTAL RESULTS

To examine our RSP scheme qualitatively, we compare the theoretically predicted probability distribution of the remotely prepared states with the experimental data taken using the ICCD camera, with the wave plates set at different angles. Figure 2(c) shows the *joint* probability distribution of the remotely prepared states of photon B. All images are captured in the far field of the SPDC source, and a so-called sector hologram for projecting onto the $|v_\ell\rangle$ is displayed on the SLM. The sector hologram is generated by imprinting the corresponding phase distribution of $|v_\ell\rangle = -i(|+\ell\rangle - |-\ell\rangle)/\sqrt{2} \propto \sin(\ell\varphi)$ state onto a normal blazed grating, i.e., $\mathrm{mod}(\mathrm{sgn}(\sin(\ell\varphi)) + 2\pi x/\Lambda, 2\pi)$ where mod is the modulo function that gives the remainder of the first argument divided by the second one, sgn is the sign function, and Λ and x are the grating pitch and the Cartesian coordinate, respectively. Apart from contrast quality, the theoretical predictions Fig. 2(b) and the experimental data Fig. 2(c) are in very good agreement. We can also rule out superpositions of higher order p modes, because the SMF used for triggering the ICCD camera filters the photons from higher order p modes.

For completeness we also measure the fidelity in order to estimate the quality of the teleportation scheme by performing quantum state tomography on the remotely prepared states. We use projections onto states from mutually unbiased bases (MUBs) for a bidimensional Hilbert space $\{|+\ell\rangle, |-\ell\rangle\}$. The measurements consist of projections onto states from the set $\{h_\ell, v_\ell, a_\ell, d_\ell, l_\ell, r_\ell\}$, where the index ℓ represents the OAM working subspace [28,29]. These states are eigenstates of the Pauli matrices. The density matrix of the state can be reconstructed from these measurements using the maximum

TABLE I. Measured fidelity F of different prepared states in the OAM subspace of $|\ell| = 2$. Errors are calculated using Monte Carlo simulation with Poissonian distribution of counting statistics.

Initial polarization state	Teleported state to Bob	F
$\vert L\rangle$	$\vert +2\rangle$	0.995 ± 0.003
$\vert V\rangle$	$\vert v_2\rangle$	0.994 ± 0.004
$\vert D\rangle$	$\vert d_2\rangle$	0.984 ± 0.008
$\vert H\rangle$	$\vert h_2\rangle$	0.999 ± 0.002
$\vert A\rangle$	$\vert a_2\rangle$	0.992 ± 0.013
$\vert R\rangle$	$\vert -2\rangle$	0.999 ± 0.001

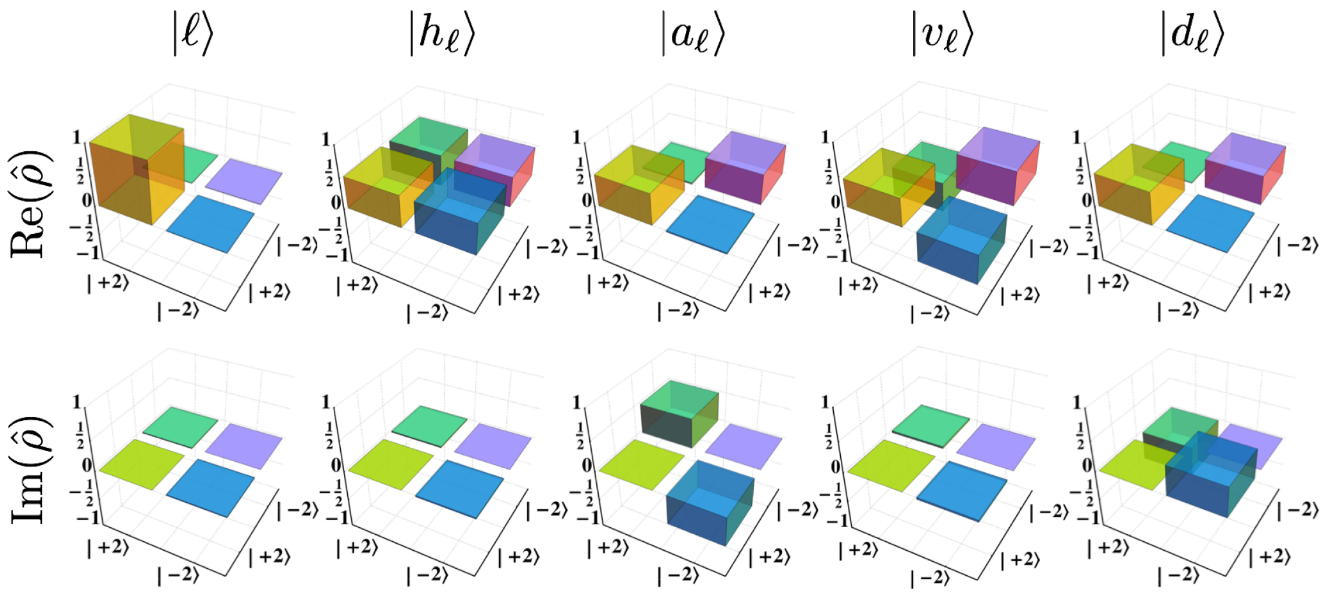

FIG. 3. (Color online) Real (upper row) and imaginary (lower row) parts of the reconstructed density matrices for the prepared states in OAM subspace of $|\ell| = 2$ shown in Fig. 2. The density matrices are reconstructed via quantum state tomography, where projections over six eigenstates of Pauli matrices are used to estimate the four real parameters that specify the density matrix.

likelihood estimate [30]. To perform these projective measurements conditioned by "clicks" on the detector A, we replaced the ICCD camera with a second SLM followed by a SMF and a second APD (the delay line is no longer necessary). The coincidence counts between the two detectors are measured by a coincidence box with a time window of 10 ns. The second SLM on arm B projects the photons onto one of the aforementioned states. The density matrices corresponding to the different remotely prepared states are reconstructed via this *overcomplete* set of measurements. All coincidence counts for reconstructing the density matrices are averaged over 100 s.

The density matrices for the different remotely prepared states are shown in Fig. 3. The key performance indicator of successful RSP is the state fidelity, defined as $F = (\mathrm{Tr}\sqrt{\sqrt{\hat{\rho}}\hat{\rho}_r\sqrt{\hat{\rho}}})^2$, where $\hat{\rho}_r$ and $\hat{\rho}$ are the reconstructed and theoretical density matrices, respectively. Fidelities of different remotely prepared states are reported in Table I. All fidelities are above 98.4%, indicating the very high quality of the remotely prepared states and therefore validating this RSP scheme.

IV. CONCLUSION

In summary, we have experimentally shown that it is possible to remotely prepare a generally known quantum state from the spin angular momentum space of a single photon onto an OAM subspace. The very high fidelities of the RSP scheme and the relatively simple experimental technique required with an efficiency approaching 100% make this specific scheme very promising for quantum key distribution, and in general for quantum cryptography. Our work also opens the possibility to use OAM of photons in different quantum computing applications. Either as qudits in the computing process itself or as a connecting system between optical quantum computers, driven by photons with polarization encoded qubits, and photonic quantum memories [31].

ACKNOWLEDGMENTS

The authors thank Filippo Cardano and Jeremy Upham for fruitful discussions, and acknowledge the support of the Canada Excellence Research Chairs (CERC) Program.

[1] A. Einstein, B. Podolsky, and N. Rosen, Phys. Rev. **47**, 777 (1935).
[2] L. Hardy, Phys. Rev. Lett. **71**, 1665 (1993).
[3] A. J. Leggett, Found. Phys. **33**, 1469 (2003).
[4] C. H. Bennett, G. Brassard, C. Crépeau, R. Jozsa, A. Peres, and W. K. Wootters, Phys. Rev. Lett. **70**, 1895 (1993).
[5] C. H. Bennett, D. P. DiVincenzo, P. W. Shor, J. A. Smolin, B. M. Terhal, and W. K. Wootters, Phys. Rev. Lett. **87**, 077902 (2001).
[6] D. Boschi, S. Branca, F. DeMartini, L. Hardy, and S. Popescu, Phys. Rev. Lett. **80**, 1121 (1998).
[7] J. T. Barreiro, T.-C. Wei, and P. G. Kwiat, Phys. Rev. Lett. **105**, 030407 (2010).
[8] D. Bouwmeester *et al.*, Nature (London) **390**, 575 (1997).
[9] J. T. Barreiro, N. K. Langford, N. A. Peters, and P. G. Kwiat, Phys. Rev. Lett. **95**, 260501 (2005).
[10] J. T. Barreiro, T.-C. Wei, and P. G. Kwiat, Nat. Phys. **4**, 282 (2008).
[11] V. D'Ambrosio *et al.*, Nat. Commun. **4**, 2432 (2013).
[12] X. Wang *et al.*, Nature (London) **518**, 516 (2015).
[13] E. Karimi, D. Giovannini, E. Bolduc, N. Bent, F. M. Miatto, M. J. Padgett, and R. W. Boyd, Phys. Rev. A **89**, 013829 (2014).
[14] A. Z. Khoury and P. Milman, Phys. Rev. A **83**, 060301 (2011).
[15] L. Chen and W. She, Phys. Rev. A **80**, 063831 (2009).

[16] S. Franke-Arnold, S. M. Barnett, M. J. Padgett, and L. Allen, Phys. Rev. A **65**, 033823 (2002).
[17] S. P. Walborn, A. N. deOliveira, R. S. Thebaldi, and C. H. Monken, Phys. Rev. A **69**, 023811 (2004).
[18] A. Mair *et al.*, Nature (London) **412**, 313 (2001).
[19] M. Padgett and J. Courtial, Opt. Lett. **24**, 430 (1999).
[20] S. Slussarenko *et al.*, Opt. Express **18**, 27205 (2010).
[21] N. González, G. Molina-Terriza, and J. P. Torres, Opt. Express **14**, 9093 (2006).
[22] M. J. Padgett and J. P. Lesso, J. Mod. Opt. **46**, 175 (1999).
[23] L. Marrucci *et al.*, J. Opt. **13**, 064001 (2011).
[24] J. Calsamiglia and N. Lütkenhaus, Appl. Phys. B **72**, 67 (2001).
[25] P. G. Kwiat and H. Weinfurter, Phys. Rev. A **58**, R2623 (1998).
[26] R. Fickler *et al.*, Sci. Rep. **3**, 1914 (2013).
[27] R. S. Aspden *et al.*, New J. Phys. **15**, 073032 (2013).
[28] B. Jack *et al.*, New J. Phys. **11**, 103024 (2009).
[29] E. Nagali *et al.*, Opt. Express **17**, 18745 (2009).
[30] D. F. V. James, P. G. Kwiat, W. J. Munro, and A. G. White, Phys. Rev. A **64**, 052312 (2001).
[31] A. Nicolas *et al.*, Nat. Photon. **8**, 234 (2014).